PHYSICAL REVIEW B VOLUME 46, NUMBER 21 1 DECEMBER 1992-I

Phase transitions in multilayer helium films

E. Cheng
Department of Physics, Ohio State University, Columbus, Ohio 43210

Milton W. Cole
Department of Physics, Pennsylvania State University, University Park, Pennsylvania 16802

W. F. Saam
Department of Physics, Ohio State University, Columbus, Ohio 43210

Jacques Treiner
Division de Physique Théorique, Institut de Physique Nucléaire, F-91406 Orsay CEDEX, France

(Received 2 March 1992)

Multilayer helium films have, until recently, been predicted and observed to exhibit a standard form of structural behavior: one or two solid layers reside adjacent to the substrate and continuous wetting liquid extends outward thereafter. We report contrary theoretical results in the case of weak-binding surfaces, the alkali metals and H_2 being particularly important examples. Depending on the substrate potential, the predicted behavior can be either nonwetting or prewetting. The focus is on ^{4}He, but some results for ^{3}He are presented. Compound substrates, helium layer solidification, third sound, superfluid onset, and possible phase diagrams for $T>0$ are discussed. The calculations utilize semiempirical density-functional methods which have proven to be accurate in other applications. Recent experiments with alkali metals and H_2 are discussed in relation to theoretical results.

I. INTRODUCTION

Helium films have been extraordinarily fascinating subjects for more than 50 years.[1-3] Originally, their thermal and mass flow properties attracted interest as manifestations of ^{4}He bulk superfluidity. More recently, attention has been drawn to these films as convenient probes of van der Waals (VDW) forces,[4-6] as examples of topological long-range order[7] (exhibiting a vortex-mediated Bose superfluid transition), as an example of a quasi-two-dimensional (2D) magnetic solid or Fermi superfluid,[8,9] and as a system exhibiting liquid-solid layering transitions[10,11] *inter alia.* We predict in this paper other kinds of phase-transition behavior, which we expect for appropriate substrates. Both pure and isotopic mixture films are discussed.

A "standard model" of He adsorption has been invoked traditionally to interpret extant data.[2] We describe it now and take exception to it below. The model describes the film's compression in the attractive potential $V(r)$ provided by the substrate.[12] This potential is deemed sufficient to solidify one or more film layers. Higher coverage films wet the substrate continuously. The film thickness d is related to the thermodynamic conditions (pressure p, chemical potential μ, and temperature T), by the relation[4,6,13]

$$\Delta\mu=\mu-\mu_0 , \tag{1.1}$$

$$\Delta\mu=kT\ln(p/p_0)=f(d) , \tag{1.2}$$

where μ_0 and p_0 correspond to bulk He, k is Boltzmann's constant, and $f(d)$ is related to the asymptotic substrate potential. In the regime where retardation of the VDW force can be neglected,[14]

$$f(d)\simeq-\Delta C_3/d^3 , \tag{1.3}$$

where

$$\Delta C_3=C_3-C_3^{\rm He} . \tag{1.4}$$

C_3 is the coefficient of the (nonretarded) VDW potential provided by the substrate

$$V(z)\sim-C_3/z^3 \tag{1.5}$$

and $C_3^{\rm He}$ is the coefficient of a hypothetical He "substrate." Here z is the surface-normal coordinate. Equation (1.2) has been confirmed in at least one set of experiments over an extended range of d, including retardation.[5]

This standard model perceives the substrate as a nucleation center for the adsorption process. While not usually stated explicitly, this view is based on the belief that He, the *most* inert and least polarizable gas, will be preferentially attracted to any material other than itself.[15] An explicit calculation that demonstrates this can be done; the following heuristic discussion is an example. The most frequently used derivation of the adsorption potential is based on a sum of two-body interactions[16] between the He atom at $\mathbf{r}$ and the substrate atoms at $\mathbf{R}_i$

$$V(\mathbf{r})\simeq\sum_i u(\mathbf{r}-\mathbf{R}_i) , \tag{1.6}$$

where one commonly assumes a Lennard-Jones (LJ) pair potential

$$u(x)=4\epsilon[(\sigma/x)^{12}-(\sigma/x)^{6}] \tag{1.7}$$

and the combining rules[17–19]

$$\epsilon=[\epsilon_{\mathrm{He}}\epsilon_{\mathrm{sub}}]^{1/2}\ ,\quad \sigma=(\sigma_{\mathrm{He}}+\sigma_{\mathrm{sub}})/2\ , \tag{1.8}$$

where the subscripts denote well depths $\epsilon_{\mathrm{He}}(\epsilon_{\mathrm{sub}})$ and hard-core diameters $\sigma_{\mathrm{He}}(\sigma_{\mathrm{sub}})$ for the He-He (substrate-substrate) interatomic potential. Since the adsorption potential-well depth (D) is typically[20] 5ε, and since $\epsilon_{\mathrm{sub}}>\epsilon_{\mathrm{He}}$, this analysis yields well depths $D\geq 5\epsilon_{\mathrm{He}}\simeq 50$ K. The resulting binding energy E_b greatly exceeds the cohesive energy $|\mu_0|=7.17$ K of liquid ^{4}He; the film's compression, solidification, and wetting behaviors follow as plausible consequences.

The preceding argument has one *major* flaw, with qualitative implications for the conclusion: a substantial error can arise from use of the combining rule (1.8). When the ionization energies of the interacting atoms differ by a large factor, the discrepancy in ε can be as much as a factor of 10.[19] For alkali-metal-atom–noble-gas-atom interactions this can be interpreted in terms of the anomalously large equilibrium separation due to the weakly bound valence electron.[21] As a consequence, the *pair* well depth is less than or of order one-half of that of the noble-gas atom interacting with its own kind.[19,22] An alternative route to the same (qualitative) conclusion is to derive $V(r)$ from a collective, many-body theory of the substrate's electronic response to an adatom.[12,16] The well depths that result can be quite shallow; see Fig. 1, which displays only the small D cases of adsorption. One observes that D can be comparable to $|\mu_0|$ in some weak-binding cases. In such instances, the "standard model" of adsorption behavior is totally inappropriate. Qualitatively distinct phenomena are expected to occur, as described below.

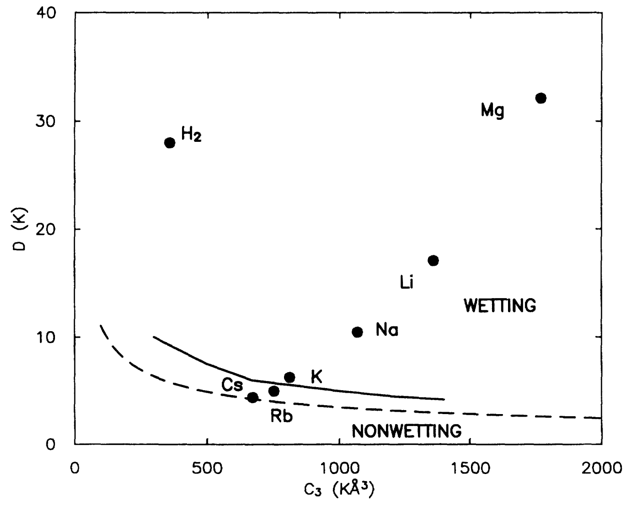

FIG. 1. Phase diagram of ^{4}He adsorption on weak-binding substrates. Each point corresponds to a substrate potential characterized by well depth D and van der Waals coefficient C_3; values are selected from those reported in Ref. 12. Estimated uncertainties are 30% and 10%, respectively. The solid curve is the wetting-nonwetting boundary predicted from the nonlocal density-functional theory. The dashed curve uses the more simplistic estimate, based on Eqs. (2.1) and (2.3).

The organization of this paper is as follows. Section II treats ^{4}He adsorption, using a density-functional model.[23,24] This leads in some cases to wetting behavior, including the possibility of a *prewetting* transition.[25] Prewetting, a discontinuous jump in coverage, has been predicted, but not yet observed, for classical gases.[15,26–30] It turns out to be more readily observable for He than for classical films and in fact may have been observed in recent experiments of Shirron and Mochel[31] on ^{4}He adsorbed on H_2. *Nonwetting* is predicted in other cases; for the most favorable weak-binding case of ^{4}He on Cs, our prediction of nonwetting has been very recently verified by Nacher and Dupont-Roc, and by Mukherjee, Druist, and Chan.[32] Other recent work by Ketola, Wang, and Hallock[33] using third sound shows a large, approximately ten-layer prewetting jump for ^{4}He on Cs. This prewetting jump and subsequent wetting are suggested to be induced by Cs surface roughness, a scenario which is consistent with ^{4}He nonwetting on a smooth Cs substrate.

The primary focus of Sec. III is on the low-temperature adsorption of ^{4}He on simple substrates. A number of other issues are addressed, however. These include ^{4}He adsorption on common substrates such as graphite plated with several layers of alkali metals, estimates of substrate potential strengths required to solidify either one or two layers of adsorbed ^{4}He, third sound, superfluid onset, and possible phase diagrams for $T>0$. Finally, comparisons with available experimental data are given.

Section III examines wetting of ^{3}He on weak-binding substrates. The results are less complete in this case, but show qualitatively similar features. A difference for ^{3}He is the possibility of a prewetting transition between a 2D superfluid gas phase and a multilayer liquid.

Section IV summarizes our results. Some aspects of the present theory have been described previously in short communications.[34–37]

II. ^{4}HE FILMS

A. Introduction

In this section we use density-functional theory to calculate the equilibrium properties of zero-temperature ^{4}He films adsorbed on weak-binding substrates such as the alkali metals and H_2. Our quantitative analysis uses a nonlocal functional developed by Dupont-Roc *et al.*[23] and used in a study of helium mixture films.[24] Qualitatively, the key physics of wetting versus nonwetting may be understood from a simple estimate of the energy balance when a film is deposited on a surface. The gain in energy per unit area of a thick film due to the attraction of the substrate is of the order of the integral of $\rho(z)V(z)$, where $V(z)$ is the external potential due to the substrate, which occupies the half space $z\leq 0$, and where $\rho(z)$ is the film atomic number density. The cost in energy is that due to the creation of two interfaces in the film and is of the order of twice the liquid-vapor surface tension σ_{lv}. Hence, an approximate criterion for nonwetting is

$$\sigma_{\mathrm{lv}}\geq -\tfrac{1}{2}\rho_0\int_{z_{\mathrm{min}}}^{\infty} V(z)dz\ , \tag{2.1}$$

where we approximate $\rho(z)$ by the bulk ^{4}He density ρ_0 at zero temperature and pressure, and $z_{\min}$ is the position of the minimum of $V(z)$. For specificity we employ the Lennard-Jones potential due to a planar substrate

$$V(z)=\left[\frac{4C_3^3}{27D^2}\right]\frac{1}{z^9}-\frac{C_3}{z^3}\,, \tag{2.2}$$

where, as above, D is the well depth and C_3 the VDW coefficient. Combination of Eqs. (2.1) and (2.2) yields, with the appropriate ^{4}He parameters,

$$(C_3D^2)^{1/3}\leq 3.33\sigma_{\mathrm{lv}}/\rho_0=43\ \mathrm{K\,\AA} \tag{2.3}$$

as our approximate condition for nonwetting. This is plotted as the dashed boundary in Fig. 1; we shall see that it compares surprisingly well to the results of the full theory.

B. A simple model

The analysis of Eq. (2.1) can be improved upon by use of a simple phenomenological model which permits examination of the prewetting transition sheet[38] emerging from the wetting-nonwetting boundary. Assume that the film has thickness l and uniform density ρ, that the gradient energy due to the presence of surfaces varies exponentially from zero at $l=0$ to $(1+\delta)\sigma_{\mathrm{lv}}$ over a characteristic length ζ, and that the repulsive core of the potential limits the approach of the film to a distance ξ from the substrate, where $\xi=(2C_3/3D)^{1/3}$ is the position of the minimum of $V(z)$. Then

$$\sigma(l,\Delta\mu)=\sigma_{w0}+\sigma_{\mathrm{lv}}(1+\delta)(1-e^{-l/\zeta})+\int_{\xi}^{\xi+l}dz\,\rho V(z)-\rho l\Delta\mu\,, \tag{2.4}$$

where σ_{w0} is the bare substrate surface energy. Inputting Eq. (2.2), we rewrite Eq. (2.4) in terms of the dimensionless variables

$$\delta\sigma(x,h)=\frac{\sigma(l,\Delta\mu)-\sigma(\infty,0)}{\rho D\xi}\,,$$

$x=l/\xi$, $\beta=\xi/\zeta$, and $h=+\Delta\mu/D$ as

$$\delta\sigma(x,h)=-\alpha e^{-\beta x}+\frac{3}{4(1+x)^2}-\frac{1}{16(1+x)^8}-xh\,, \tag{2.5}$$

$$\alpha\equiv\frac{(1+\delta)\sigma_{\mathrm{lv}}}{\rho D\xi}=\frac{(1+\delta)\sigma_{\mathrm{lv}}}{\rho(\frac{2}{3}C_3D^2)^{1/3}}\,. \tag{2.6}$$

The model specified by Eq. (2.5) has phase diagrams in α-h space which depend in important ways upon β.[39] For $\beta>2.2$ (or $\zeta<\xi/2.2$) the behavior is most similar to that found in Sec. II C using the full nonlocal density-functional theory.[39] Large β indicates that the energy cost of forming film surfaces reaches its limit rather rapidly with increasing thickness. We choose $\beta=3$ for purposes of illustration.

To examine wetting versus nonwetting we set $h=0$, placing us at liquid-gas coexistence, and we search for the minimum of $\delta\sigma(x,0)$ as a function of x. Straightforward

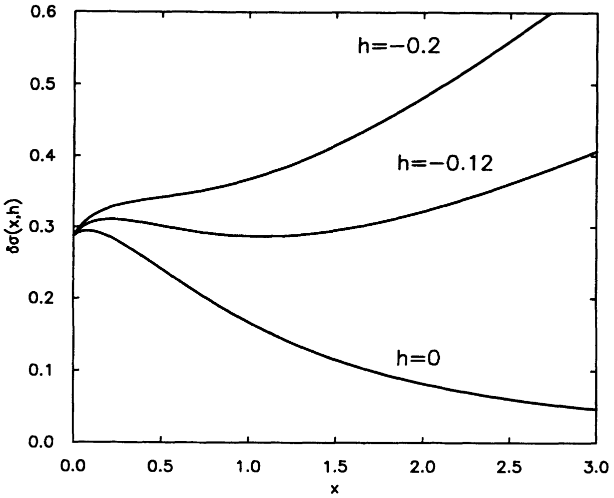

FIG. 2. Prediction of the simple model, Eq. (2.5), with $\beta=3$ for the dimensionless excess surface tension as a function of film thickness (measured in units of the adatom equilibrium distance). From top to bottom, the curves are for values -0.2, -0.120, and 0 of the field h. These correspond to cases of a wetting film at coexistence, a prewetting transition, and a zero thickness unsaturated film, respectively, as discussed in the text.

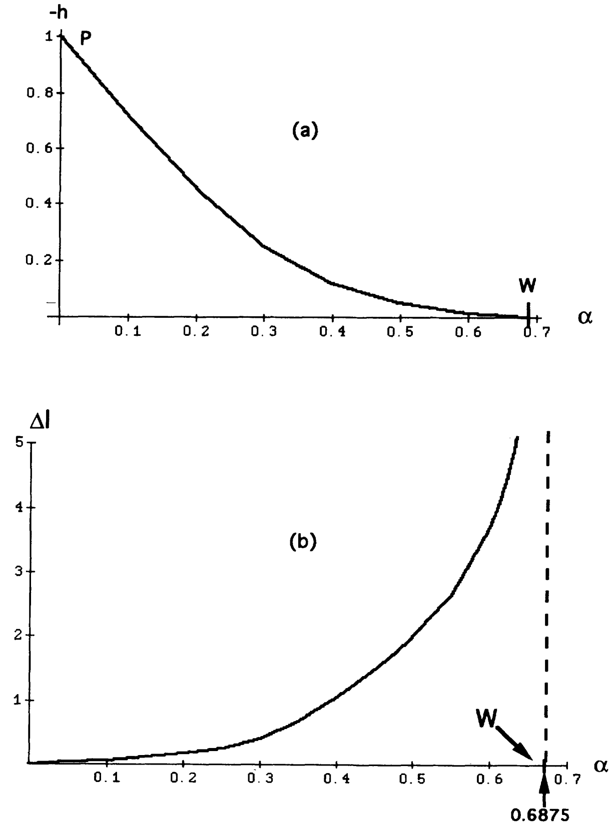

FIG. 3. Predictions of the simple model for $\beta=3$: (a) the phase diagram in α-h space with the prewetting line PW and wetting transition point W, and (b) the film thickness jump Δl (in units of the adatom equilibrium distance) along PW.

analysis shows that the minimum occurs at $x=0$ for $\alpha > \frac{11}{16}=0.6875$ and at $x=\infty$ for $a<\frac{11}{16}$, so that the condition $\alpha=\frac{11}{16}$ determines the wetting-nonwetting boundary. This condition is precisely the same as that of Eq. (2.3) with the choice $\delta=1.0$. In the range $0<\alpha<\frac{11}{16}$, wetting occurs via a prewetting transition,[25] characterized by a film thickness jump from $l=0$ to a thickness Δl. Plots of $\delta\sigma(x,h)$ are shown in Fig. 2 for three values of h. These are $h=0$ (coexistence), $h=-0.120$ (at the prewetting transition where there are equal minima at $l=0$ and at $l=\Delta l=1.066\xi$), and $h=-0.2$ (where the equilibrium film thickness is zero). Figure 3(a) shows the phase diagram in α-h space with the prewetting line *PW* and the wetting transition point *W* indicated. The film thickness jump along *PW* is plotted in Fig. 3(b). We shall see that the predictions of this simple model are qualitatively consistent with those of the next section. Note that the wetting transition terminating the prewetting line is driven by changes in α, rather than by the temperature.[25]

C. Nonlocal density-functional theory

Now we address the physics of ^{4}He films quantitatively within the nonlocal density-functional theory of Dupont-Roc *et al.*[23] Our treatment is restricted to $T=0$, and our substrate is translationally invariant parallel to the liquid-solid interface[40]; thus we assume any ^{4}He film to be completely superfluid. The ^{4}He functional embodies a nonlocal generalization of the Skyrme[41] formalism introduced in nuclear physics and is similar in spirit to the work of Tarazona[42] for classical fluids. It has the form

$$E_4=\int d\mathbf{r}\, H_{\rm nl}(\rho,\nabla\rho)\ , \tag{2.7}$$

$$H_{\rm nl}=\frac{\hbar^2}{2m}|\nabla\phi|^2+\tfrac{1}{2}\int d\mathbf{r}'[\rho(\mathbf{r})\rho(\mathbf{r}')V_l(|\mathbf{r}-\mathbf{r}'|)] + \frac{c}{2}\rho(\mathbf{r})(\bar{\rho}_{\mathbf{r}})^{1+\gamma}\ , \tag{2.8}$$

where v_l is the standard Lennard-Jones ^{4}He-^{4}He interaction potential, screened at distances shorter than a characteristic length h,

$$V_l(R)=4\epsilon\left[\left[\frac{\sigma}{R}\right]^{12}-\left[\frac{\sigma}{R}\right]^{6}\right] \quad \text{for } R\geq h\ , \tag{2.9}$$

$$V_l(R)=V_l(h)\left[\frac{R}{h}\right]^4 \quad \text{for} R<h\ . \tag{2.10}$$

Finally, $\phi(\mathbf{r})=\sqrt{\rho(\mathbf{r})}$, and m is the atomic mass.

The $\bar{\rho}_{\mathbf{r}}$ in Eq. (2.5) is the "coarse-grained density," defined by averaging $\rho(\mathbf{r})$ over a sphere with radius $h=2.377$ Å. With the parameters $\epsilon=10.22$ K, $\sigma=2.556$ Å, $c=1.045\,54\times10^7$ K Å$^{3(1+\delta)}$, and $\gamma=2.8$,[23] this model accurately reproduces the equation of state, surface tension, and static density-density response function of bulk liquid ^{4}He.

It is straightforward to apply the above model to the problem of thin liquid ^{4}He films adsorbed on a substrate surface by including the contribution of the substrate potential $V(z)$ to the total density functional. The energy per unit area of the film is now

$$\epsilon=\frac{1}{A}\int d\mathbf{r}\, H(\rho,\nabla\rho)=\frac{E_4}{A}+\int dz\,\rho(z)V(z)\ , \tag{2.11}$$

where $V(z)$ is given by Eq. (2.2), and A is the surface area.

The film density profile is determined by the Euler equation

$$\mu=\delta\epsilon/\delta\rho(z)\ . \tag{2.12}$$

This equation can be integrated numerically to obtain the film profile at any chemical potential μ for any surface characterized by C_3 and D. A further integration gives the film coverage n per unit area (or a corresponding film thickness l, in nominal "layers") and the surface free energy σ (per unit area),

$$l\equiv\frac{n}{\rho_0^{2/3}}=\frac{1}{\rho_0^{2/3}}\int_0^\infty dz\,\rho(z)\ , \tag{2.13}$$

$$\sigma=\epsilon-\mu n\ . \tag{2.14}$$

The explicit form of the Euler equation is given by the integro-differential equation

$$-\frac{\hbar^2}{2m}\frac{d^2\phi(z)}{dz^2}+[U_{\rm nl}(z)+V(z)]\phi(z)=\mu\phi(z)\ , \tag{2.15}$$

$$\begin{aligned}U_{\rm nl}(z)={}&4\pi\epsilon\sigma^2\left\{\int_{-\infty}^{z-h}+\int_{z+h}^{\infty}\right\}dz'\rho(z')\left[\frac{1}{5}\left[\frac{\sigma}{z-z'}\right]^6-\frac{1}{2}\right]\left[\frac{\sigma}{z-z'}\right]^4\\&+4\pi\epsilon\sigma^2\int_{z-h}^{z+h}dz'\rho(z')\left\{\left[\frac{8}{15}\left[\frac{\sigma}{h}\right]^6-\frac{5}{6}\right]-\frac{1}{3}\left[\left[\frac{\sigma}{h}\right]^6-1\right]\left[\frac{z-z'}{h}\right]^6\right\}\left[\frac{\sigma}{h}\right]^4\\&+\frac{3c}{8h}(1+\gamma)\int_{z-h}^{z+h}dz'\left\{\left[1-\left[\frac{z-z'}{h}\right]^2\right]\rho(z')(\bar{\rho}_{z'})^{\gamma}+\frac{c}{2}(\bar{\rho}_z)^{1+\gamma}\right\}\ .\end{aligned} \tag{2.16}$$

In the low-coverage limit the self-consistent mean field $U_{\rm nl}(z)$ is negligible so that Eq. (2.15) becomes the Schrödinger equation for a single ^{4}He atom in $V(z)$, and the density profile is proportional to the square of the ground-state wave function of this equation. The coverage thus approaches zero in the limit that $\mu\rightarrow-\epsilon_b$ from above, where ϵ_b is the single-atom binding energy in $V(z)$.

For a given $V(z)$, and fixed coverage, we numerically solve Eq. (2.15) as an eigenvalue problem with the self-consistent iteration method described in Ref. 23. The density profile $\rho(z)=\phi^2(z)$ and the eigenvalue μ emerge from the computation. Typical profiles for the wetting (with prewetting) case are shown in Fig. 4. Note that the nonlocal theory predicts a rich layering structure in the profiles near the substrate surface. This structure should be indirectly observable in third sound experiments, as discussed later.

Figure 1 shows the predicted wetting-nonwetting boundary. Note the remarkable agreement between this boundary and the simple prediction of Eq. (2.3), or equivalently, of the simple model of Eq. (2.4). Further, this boundary is the terminus, at $\Delta\mu=0$, of the prewetting sheet in $C_3-D-\Delta\mu$ space shown in Fig. 5.[25] In Fig. 6 we show the prewetting coverage jump Δl as a function of D as the prewetting sheet is crossed at fixed C_3, as obtained from the nonlocal theory. Note that Δl appears to saturate at 0.4 layers (0.032 Å^{-2}) for large D. For the simple model Δl does not saturate as $D\rightarrow\infty$ ($\alpha\rightarrow 0$) since the model does not correctly reflect the 2D limit. This saturation is actually expected since large D renders the first-layer region essentially two dimensional, and 2D ^{4}He is known to undergo a liquid-gas transition.[43] In fact, we find a 2D liquid-gas transition within the present model; its reduction to 2D is obtained by noting that, for a uniform 2D density ρ_{2D}, one has $\rho=\rho_{2D}\delta(z)$. Substituting this in Eq. (2.7) leads to a grand free energy per unit area ω given by

$$\omega=\frac{4\pi\epsilon\sigma^2}{3}\left[\frac{8}{5}\left[\frac{\sigma}{h}\right]^{10}-\frac{5}{2}\left[\frac{\sigma}{h}\right]^{4}\right]\rho_{2D}^2 + c\left[\frac{3}{4h}\right]^{1+\gamma}\rho_{2D}^{2+\gamma}-\mu\rho_{2D} \; . \tag{2.17}$$

This predicts, via minimization at constant μ, liquid-vapor coexistence with zero vapor density, zero pressure, $\mu=-0.18$ K, and a liquid density of $\rho_{2D}=0.026$ Å^{-2}. The slightly larger value of $n=0.032$ Å^{-2} that we obtain with the full nonlocal theory apparently reflects the fact that very large values of D are required to accurately achieve the 2D limit. Indeed, a simple estimate based on a harmonic-oscillator[44] approximation to $V(z)$ for large D gives the results that the z motion is reduced to less than 1% of interparticle spacing in the 2D liquid for D greater than about 3600 K for $C_3=1000$ K Å^3. The difference between the actual 2D ^{4}He condensation density of 0.044 Å^{-2} (Ref. 43) and the value 0.026 Å^{-2} measures the error in our theory in the limit of extreme density gradients.

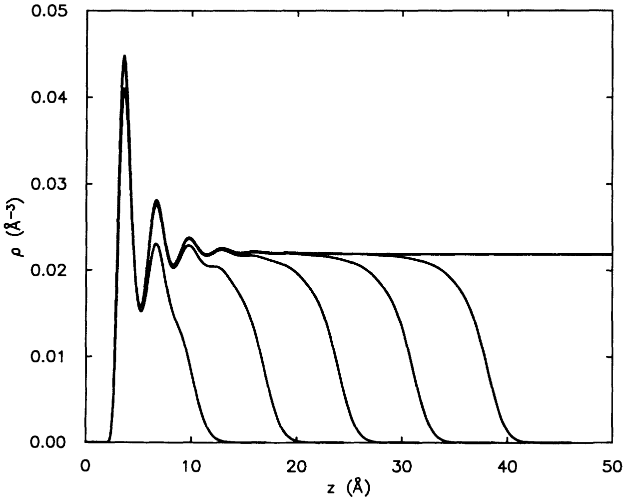

FIG. 4. Film profiles calculated from the nonlocal theory for the case $C_3=1000$ K Å^3 and $D=10$ K; note the layerlike structure. The uppermost curve reflects a thickness jump greater than eight layers associated with the prewetting transition.

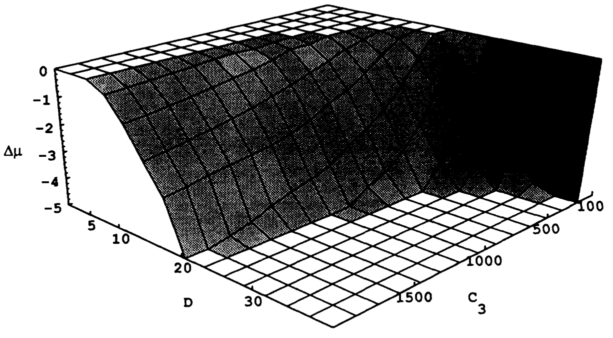

FIG. 5. Prewetting transition sheet, terminating in the wetting-nonwetting transition in the C_3-D plane. D and μ are in K, C_3 in K Å^3.

For completeness we show in Figs. 7 and 8 some computed values of the chemical potential $\mu(l)$ as a function of coverage as well as the surface free energy $\sigma(l,\Delta\mu)$ given by

$$\sigma(l,\Delta\mu)=\left[\int_0^l\Delta\mu(l')dl'-\Delta\mu l\right]\rho_0^{2/3} \; ,$$
$$\Delta\mu(l)\equiv\mu(l)-\mu_0 \; , \tag{2.18}$$

where μ_0 is the bulk ^{4}He chemical potential at coexistence. Equilibrium film thicknesses are those minimizing $\sigma(l,\Delta\mu)$ and a film thickness transition occurs when

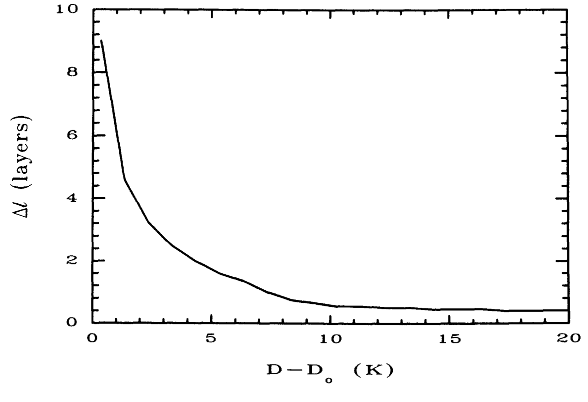

FIG. 6. Prewetting transition thickness discontinuity as a function of well-depth excess relative to the critical value, $D_0=9.6$ K, for the case $C_3=1000$ K Å^3.

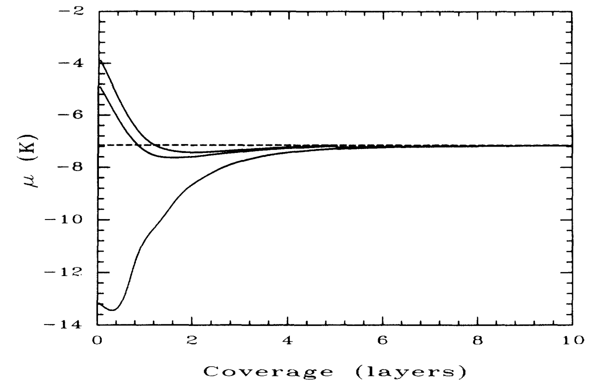

FIG. 7. The chemical potential $\mu(l)$ at $C_3 = 1000$ K Å^3 for, from bottom to top, $D = 22.5$, 10.5, and 8.5 K.

$\sigma(l,\Delta\mu)$ has equal minima. [A Maxwell equal-area construction on $\mu(l)$ is equivalent]. In Fig. 8 we show $\sigma(l,0)$ for, from top to bottom, a case of nonwetting and two cases of wetting (which have prewetting transitions at $\Delta\mu < 0$). For large l, $\sigma(l,0) - \sigma(\infty,0) = \Delta C_3 \rho_0^{5/3}/2l^2$ is determined by the difference in van der Waals coefficients.[30]

Key predictions of this work include the wetting behavior of ^{4}He on real weak-binding substrates. Points corresponding to such substrates, with values of C_3 and D from Refs. 12 and 34, are plotted in Fig. 1. The alkali metals Cs, Rb, and K are in the nonwetting regime, while Na is close to the transition line in the wetting regime. In the nonwetting regime contact angles of ^{4}He droplets can be found from Young's equation,

$$\cos\theta = \frac{\sigma_{\rm sv} - \sigma_{\rm sl}}{\sigma_{\rm lv}} , \tag{2.19}$$

where $\sigma_{\rm sv}$, $\sigma_{\rm sl}$, and $\sigma_{\rm lv}$ are the substrate-vapor, substrate-liquid, and liquid-vapor interfacial tensions, respectively. The right-hand side of Eq. (2.19) can be calculated readily from Eq. (2.14) at coexistence. The results for θ as well as prewetting jumps are given in Table I.

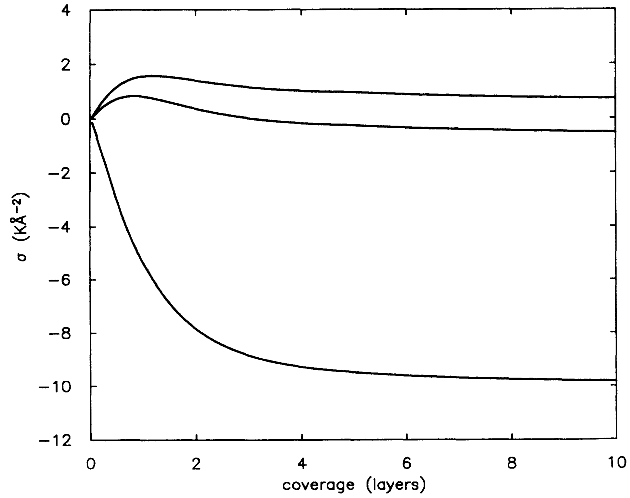

FIG. 8. The surface tension $\sigma(l)$ at $C_3 = 1000$ K Å^3 for, from bottom to top, $D = 22.5$, 10.5, and 8.5 K.

TABLE I. Contact angles θ in degrees, prewetting film thickness jumps (in layers), where relevant, and values of the potential parameters C_3 and D for the alkali metals and H$_2$ appearing in Fig. 2.

Element	θ	Δd	C_3 (K Å^3)	D (K)
Li	0°	0.80	1360	17.1
Na	0°	5.25	1070	10.4
K	73°		812	6.26
Rb	87°		754	4.99
Cs	95°		673	4.41
H$_2$	0°	0.42	360	28

Other work on thin superfluid films which is closely related to ours in terms of methodology and, in part, results is that of Krotscheck and co-workers[45] and Ji and Wortis.[46] The latter authors, in fact, explicitly vary their overall strength λ of the substrate-^{4}He potential to produce a phase diagram in $\Delta\mu - \lambda$ space possessing a wetting transition with an associated prewetting line rather like a cut through Fig. 5 at constant C_3. The results are not related to real weak-binding substrates, however. Wetting and prewetting transitions as a function of potential strength, while implicit in the work of Ref. 45, are not explored.

D. Compound substrates

The discussions above have illustrated some new and fascinating phenomena in wetting transitions. One of the most critical problems here is the availability of the weak substrates which satisfy the conditions listed above. Unfortunately, however, only three alkali-metals are predicted to show ^{4}He nonwetting. For prewetting, only Na is close enough to the transition line to have a substantial prewetting jump, as seen in Table I. Other traditionally studied substrates such as graphite and other metals have too large well depths to display nonwetting, and significant prewetting behavior is preempted by first-layer solidification phenomena.

One relatively easy way to circumvent this problem is to preplate alkali-metal layers onto these strong substrates. The resulting "compound substrate" is very likely to have a total substrate potential whose well depth is close to that of the alkali-metal overlayer (o) while the long attractive tail (C_3) is close to that of the underlying substrate (s). We write the total potential as a simple sum of two contributing parts,

$$V(z) = V_r(z) + V_a(z) , \tag{2.20}$$

$$V_r(z) = \frac{C_9^{\rm He-o}}{(z-d^o)^9} + \frac{C_9^{\rm He-s} - C_9^{\rm He-o}}{z^9} , \tag{2.21}$$

$$V_a(z) = -\frac{C_3^{\rm He-o}}{(z-d^o)^3} - \frac{C_3^{\rm He-s} - C_3^{\rm He-o}}{z^3} , \tag{2.22}$$

where V_r and V_a are, respectively, the repulsive and attractive parts of the total potential. Here we have assumed that the overlayer (of thickness d^o) continuously occupies the region $0<z\le d^o$, while the underlying substrate occupies the half space $z\le 0$.

The superposition of the potentials in Eq. (2.20) renders the total potential complicated. The attractive part, Eq. (2.20), is no longer in the familiar VDW z^{-3} form. The "effective C_3" of the total potential is no longer a constant, but a function of the overlayer thickness d^o. However, for the region $z\gg d^o$, we have

$$V_a(z)\sim -\frac{C_3^{\mathrm{He}-s}}{z^3}\ , \tag{2.23}$$

i.e., the effective C_3 is dominated by the underlying substrate.

On the other hand, the overlayer is the dominant factor in the short range (repulsive part) of the potential, which strongly affects the well depth D. For a relatively large d^o, the total short-range potential will be dominated solely by the alkali-metal overlayer. Therefore one expects a small well depth (close to that of the alkali-metals) and ^{4}He nonwetting in the cases of the heavier alkali metals. As d^o decreases, the (strong) attractive part and eventually the repulsive part of the underlying substrate potential will have its effects in the total potential and make D increase. At a critical overlayer thickness $D^o=d_c^o$, the potential well becomes attractive enough for the ^{4}He film to wet it. In situations where the overlayer thickness d^o can be continuously controlled in experiments, we expect to see a resulting compound substrate with continuously variable contact angles in the nonwetting case and continuously variable prewetting jump size in the wetting case. In Table II we list the values of d_c^o of commonly available substiates with the alkali metals for which we predict ^{4}He nonwetting. We note that the overall range of d_c^o is only several angstroms, so that only a few alkali-metal layers need to be preplated before ^{4}He no longer wets the substrate. With increasing d^o, the contact angle of the ^{4}He droplet increases, approaching the value on the bare alkali metal. We note that the above model is *not* expected to be quantitatively accurate, given its simplicity. In particular, the continuum assumption is not reliable when only a few overlayers are present. Discrete models are necessary for more accurate results.

Finally we note that it is an excellent approximation to continue using the two parameters C_3 and D to characterize the total potential. Especially for the case of predicting wetting behaviors, one can use the approximate C_3 of Eq. (2.23) and the well depth D of the total potential and the phase diagram in Fig. 2 to estimate whether the compound substrate supports wetting by ^{4}He films.

E. Layer solidification in ^{4}He films

In this section we look more carefully at the state of a helium film on a given substrate. The different situations to expect, as a function of increasing D, are the following: nonwetting, wetting with prewetting, and solidification of one or two layers. One of the most important issues in the wetting and superfluidity of ^{4}He films is to determine the substrates on which helium will solidify. It is well known, for example, that two layers solidify on graphite, while the state of the third layer, probably fluid,[47,48] is not quite clear, in the sense that it is inert with respect to observation of third sound.[49]

The approximation of translational invariance in our calculations prevents us from answering the question of solidification directly. However, one can still work out a criterion allowing us to assign a solid or a liquid character to each of the first layers. The criterion is a straightforward extension of the approach of Cheng, Ihm, and Cole[34] to the present model.

We first remark that a layer is a 2D ^{4}He system with chemical potential equal to that of the whole film. Relying on the equation of state of a 2D ^{4}He system calculated in Ref. 43, it appears that solidification in 2D occurs for a change in chemical potential of about 9K [the difference between the chemical potential at 2D solidification, 8.2 K, and that of the liquid at equilibrium, -0.8 K (Ref. 43)]. Hence if, for a given substrate, the chemical potential changes by more than 9 K during completion of a layer, then one may consider that this layer is solid. Actually one should recognize that a layer may solidify upon the addition of subsequent layers; in view of our other approximations, we shall neglect this effect. This leads us to compare the variation of the chemical potential $\Delta\mu=\mu(n_f)-\mu(n_i)$ between the coverage n_f for which a given layer reaches completion and the coverage n_i for which it starts forming. For $\Delta\mu$ larger than 9 K, solidification is likely to occur. A possible alternative criterion would be to compare the integrated density of each layer to the value of the 2D density at solidification found in Ref. 43, namely 0.0678 Å^{-2}. However, this criterion is difficult to use because a layer is a true 2D system only for very strongly attractive substrates. For weakly attractive ones, the density between maxima is not small, implying that helium atoms are able to move from one layer to the next one. Here the density criterion would still predict a solid phase because the integrated density over a layer tends to the bulk value of 0.078 Å^{-2}, which is larger than the 2D solidification density.

Figure 9 shows the variation of the chemical potential μ as a function of coverage for three different substrates: graphite, magnesium, and sodium. The case of graphite,

TABLE II. The critical overlayer thickness d_c^o (in Å) of alkali metals Cs, Rb, and K on top of various substrates.

	NaCl	Mg	Graphite	Al	Cu	Ag	Au
Cs	0.8	2.2	3.0	3.6	4.0	4.6	5.0
Rb	0.8	2.4	3.4	3.8	4.4	5.0	5.4
K	1.4	3.4	4.4	5.0	5.6	6.4	7.0

well studied experimentally, will serve as a test of our model. We have used for the helium-substrate interaction a potential of the form of Eq. (2.2) with $C_3=2088$ K Å^3 and $D=192.6$ K for graphite, $C_3=1775$ K Å^3 and $D=32.1$ K for magnesium, and $C_3=1070$ K Å^3 and $D=10.4$ K for sodium.[12] The formation of the first three layers is clearly seen on graphite, as are the first two in the case of magnesium. No such structure is seen in the case of sodium. Well-defined steps indicate well-defined layers, and the smoothing of the steps means that the layers tend to lose their individuality and will therefore be liquid rather than solid. Figure 10 shows the density profiles on graphite and on sodium, corresponding to the coverages chosen in Ref. 50. The chemical potential criterion defined above indicates that the first two layers on graphite are solid, but not the third one; this result agrees with experimental studies mentioned above.[47,48] Helium is seen to remain liquid on both sodium and magnesium.

More generally, in the C_3-D plane one can draw the lines corresponding to solidification of the first and second layers at completion; see Fig. 11. For completeness, the wetting-nonwetting line from Fig. 1 is also shown. The predictions are of course uncertain for cases close to a line; neglecting the extra compression produced by the second layer on the first one, or by the third one on the second one, may be a bad approximation here; there are also large uncertainties in the parameters of the potentials [up to ~30% on D (Ref. 12)]. Hence it may well be that the first layer does solidify on Mg, and that the second layer solidifies on MgO, Cu, and Ag. Notice that the solidification line for the first layer corresponds to values of D larger than in Ref. 34 by almost a factor of 2. We interpret this difference as reflecting the z degree of freedom, not allowed in Ref. 34, where it is assumed that a layer was a pure 2D system. In fact, a layer has a width depending on the strength of the potential. An increasing width produces a smoothing of the steps in μ, different for each substrate (see Fig. 10).

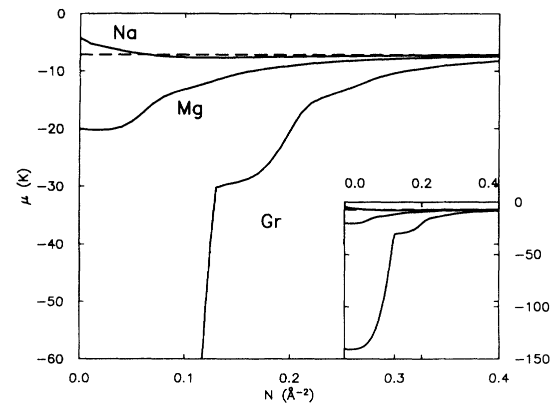

FIG. 9. The chemical potential $\mu(N)$ as a function of coverage for ^{4}He films on graphite (Gr), Na, and Mg substrates.

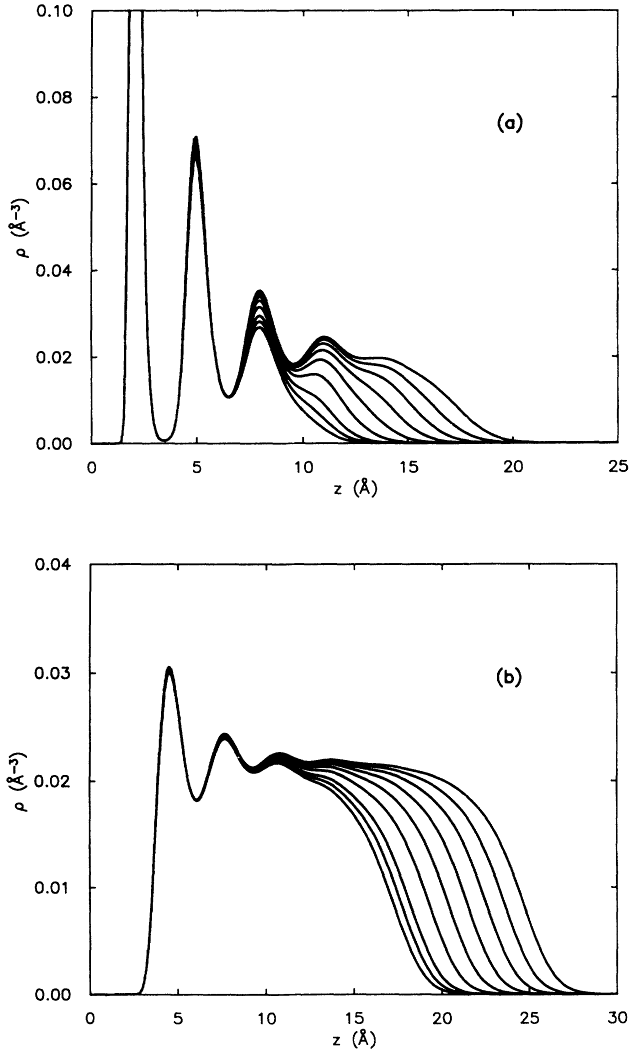

FIG. 10. Density profiles $\rho(z)$ for ^{4}He adsorbed on (a) graphite, and (b) Na for coverages (in units of Å^{-2}) of 0.294, 0.305, 0.329, 0.353, 0.377, 0.401, 0.424, and 0.448.

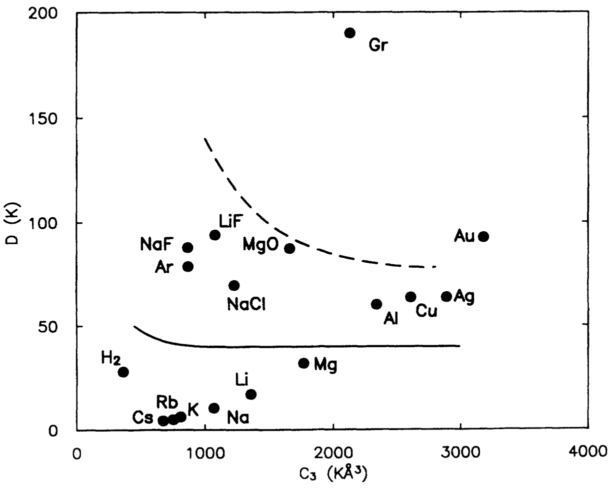

FIG. 11. Phase diagram for ^{4}He adsorption on weak-binding substrates. The lower (top) curve is the line at which the first (second) layer solidifies at completion.

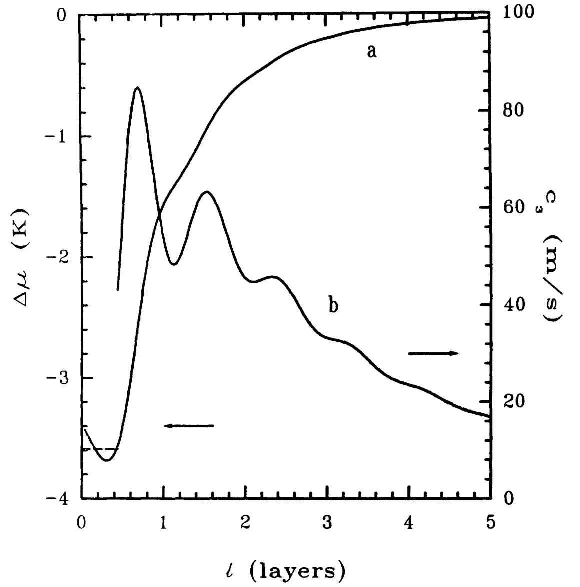

FIG. 12. Chemical potential and third-sound speed [using Eq. (2.24)] vs coverage for the values $C_3=345$ K Å^3 and $D=28$ K appropriate to ^{4}He on a solid H_2 substrate.

F. Third-sound oscillations

The oscillatory character of the density shown in Fig. 4 might well be expected to emerge in physical properties which are sensitive to film thickness. Such, indeed, is the case for the third sound velocity c_3, which is given by (see the Appendix and Ref. 51),

$$c_3^2=\frac{n_s}{m}\frac{\partial u}{\partial n}\ , \tag{2.24}$$

where n_s is the superfluid density per unit area and of the film. Using the assumption that $n_s=n$, and noting that $\mu(n)$ is a direct output of the nonlocal theory, c_3 is calculated from Eq. (2.24). For specificity we plot $\Delta\mu=\mu-\mu_0$ for the parameters appropriate to a solid H_2 substrate in Fig. 12. The density oscillations are clearly reflected in the oscillations of c_3. A detailed study of third sound on H_2-plated graphite and graphite alone will be published elsewhere.[52]

G. Superfluid onset

Our calculations for ^{4}He films have been restricted to $T=0$ and have assumed potentials translationally invariant in the plane of the substrate surface. Hence, if we restrict our considerations to regions where no solidification is expected (see Sec. II E), any film will be superfluid and could in principle be detected by third-sound experiments. For $T>0$, the films will undergo Kosterlitz-Thouless transitions to the normal state at temperatures governed by the usual relation[53]

$$T_c=\frac{n_s(T_c)\pi\hbar^2}{2mk}\approx 0.82\frac{n_s(0)\pi\hbar^2}{2mk}=1.22l\ , \tag{2.25}$$

where the factor $n_s(T_c)/n_s(0)=0.82$ is from Ref. 53. For our thinnest prewetting films (~ 0.4 layers) the transition temperature would be approximately 0.5 K. Note that this estimate is slightly below the transition temperature of 0.72 K found for 2D ^{4}He found by Ceperley and Pollack[54] using path-integral techniques.

This simple picture is rendered more complex in the presence of substrate potentials with either periodic or random character parallel to the plane of the interface.[40] In both situations the superfluid density will be less than the total density, so that a part of any liquid film will appear inert in third-sound[55] and torsional oscillator[56] experiments. Further, in both situations it is possible, depending on the interactions, to have nonsuperfluid phases[40] at $T=0$. The relevance of these phases to ^{4}He films on weak-binding substrates is being explored.

H. Phase diagrams for T > 0

It is of considerable interest to explore the temperature dependence of the wetting-nonwetting phase diagram of Fig. 5. First of all, we expect the wetting transition line at coexistence to be shifted to smaller D as thermal excitations lower the film free energy. The transition occurs when

$$\sigma_{\text{sv}}(T)=\sigma_{\text{sl}}(T)+\sigma_{\text{lv}}(T)\ . \tag{2.26}$$

At low temperature

$$\sigma_{\text{lv}}(T)=\sigma_{\text{lv}}(0)-aT^{7/3}\ , \tag{2.27}$$

where $a=6.5\times 10^{-3}$ dyn/cm K$^{7/3}$,[57] due to ripplons. The temperature-dependent corrections to $\sigma_{\text{sv}}(T)$ and $\sigma_{\text{sl}}(T)$ will vary as T^3 due to Rayleigh waves and bulk phonon reflection[58] at the wall-vapor and wall-liquid interfaces. Consequently, Eq. (2.27) provides the dominant T dependence of the wetting transition line. A substrate near this line on the nonwetting side will be wet by ^{4}He at

$$T=[\delta\sigma/a]^{3/7}\approx\left[\frac{0.2\rho_0 C_3^{1/3}\delta D}{D^{1/3}a}\right]^{3/7}\ , \tag{2.28}$$

where $\delta\sigma$ is the $T=0$ excess surface tension of a hypothetical film, i.e., the difference between the right and left sides of Eq. (2.26). The second part of Eq. (2.28) results from the use of Eq. (2.3) to estimate the dependence of $\delta\sigma$ on δD, the distance the substrate is below the wetting line at $T=0$. This prediction is actually more robust than the derivation might imply because of the stiffness of the Rayleigh (and sound) waves relative to the ripplons. Letting s be the Rayleigh wave speed, the pertinent coefficient is calculated to be

$$a_R=\sigma_R/T^3=k^3\zeta(3)/[2\pi(\hbar s)^2]\ , \tag{2.29}$$

which is of order 8×10^{-6} dyn/cm k^3, if we substitute an estimate of $s=2000$ m/sec. Hence even at $T=1$ K, the thermal contribution of the Rayleigh (and sound) waves is negligible compared to that of the ripplons, so Eq. (2.28) should be quite accurate.

Next, we consider the behavior of prewetting for $T>0$. For fixed D and C_3 we expect a phase diagram like that of Fig. 13(a). The prewetting transition at $T=0$ (Ref. 25) will have an Ising-like critical point C_a at finite temperature. For values of D such that the prewetting transition is similar to the liquid-gas transition in 2D ^{4}He (for $C_3=1000$ K Å^3, this means $D>20$ K; see Fig. 6), the critical temperature at C_a will be of the order of the $T=0$ binding energy per particle of 2D ^{4}He, or 0.8 K.[43] As the binding energy per particle (relative to its limit at zero coverage) increases with decreasing D (see Fig. 7), we anticipate that prewetting critical temperatures increase with decreasing D as well. For a case where there is nonwetting at $T=0$ but thermally induced wetting at some $T>0$, the phase diagram will look like that of Fig. 13(b). This information, collected in a more global fashion in $T-\Delta\mu-D$ space at fixed C_3 is sketched in Fig. 14. In Fig. 14, W_1W_2 is a line of wetting transitions at $T>0$ and $\Delta\mu=0$, W_1P is the $T=0$ prewetting line, and C_1C_2 is a line of prewetting critical points. P_wC_a and WC_b represent the prewetting lines shown in Figs. 13(a) and 13(b), respectively. The slope $dT/dD=\infty$ of W_1W_2 at $T=0$ can be deduced from Eq. (2.28), while the slope $d\Delta\mu/dD=0$ for W_1P at $\Delta\mu=0$ emerges from our $T=0$ computations in both the simple model of Sec. II B [see Fig. 3(a)] and the nonlocal density-functional theory. It seems likely that W_1W_2 will approach the ^{4}He liquid-gas critical point as D is reduced, with a variety of possibilities for the extension of C_1C_2 (see, e.g., Ref. 59). Note that in the context of the global picture given in Fig. 14, it seems most natural to call both WC_b and P_wC_a prewetting lines.[25]

In the above discussion we have ignored the issue of superfluid onset. However, a plausible scenario is that at some $T>0$, the prewetting film will undergo a Kosterlitz-Thouless transition at some temperature less than that of the prewetting critical point. Dashed lines of Kosterlitz-Thouless transitions in agreement with this scenario appear in Figs. 13(a) and 13(b). The corresponding sheet of Kosterlitz-Thouless transitions is not shown in Fig. 14 as it reduces the clarity of the figure. In Fig. 13 the Kosterlitz-Thouless lines do not extend into the thin-film regions. While such extensions are not in principle forbidden, further analysis[60] shows that they are not expected to occur.

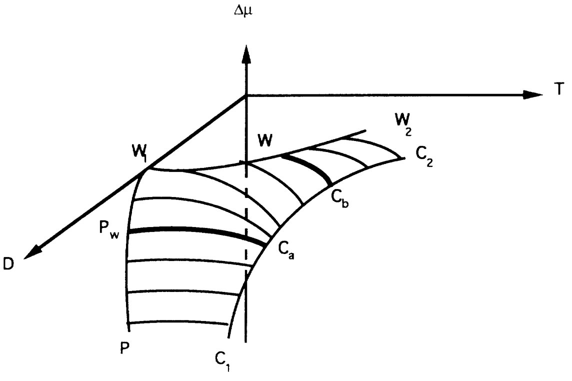

FIG. 14. Phase diagram for fixed C_3 in D-T-$\Delta\mu$ space. W_1W_2 is a line of wetting transitions at $T\geq 0$ and $\Delta\mu=0$, W_1P is the $T=0$ prewetting line, and C_1C_2 is a line of $T>0$ prewetting critical points. P_wC_a and WC_b represent the prewetting lines shown in Figs. 13(a) and 13(b), respectively.

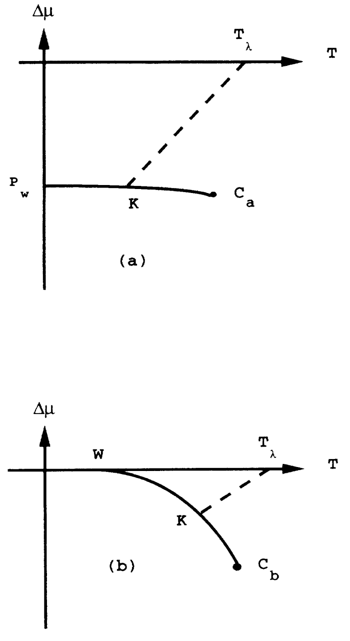

FIG. 13. Schematic phase diagrams for the cases of (a) prewetting (P_w) at $T=0$, where P_wC_a is a prewetting line ending in a critical point C_a, and (b) wetting (W) at $T>0$, where WC_b is a prewetting line ending in a critical point C_b. In both cases K-T_λ is a line of superfluid transitions.

A generalization of our density-functional theory to the $T>0$ case would provide, in principle, one means of explicitly calculating phase diagrams such as those sketched in Fig. 13. Such an approach would require at least two order parameters to properly account for both normal and superfluid densities.

I. Comparisons with experiments

Quite recently experimental work designed to test our predictions concerning ^{4}He wetting and nonwetting of the alkali metals has been performed.[61,32,33] Observations by Nacher and Dupont-Roc[61] of heat flow in ^{4}He films in a glass tube, with and without an interior cesium ring, show that ^{4}He does not wet cesium, in agreement with our predictions [see Fig. 1]. Very recent volumetric vapor pressure isotherm measurements by Mukherjee, Druist, and Chan[32] indicate a complete absence of ^{4}He adsorption on cesium-coated graphite for temperatures $T\lesssim 2$ K. This result is in agreement with our prediction and with the Nacher and Dupont-Roc[61] observations; it does, however, go farther in that it measures a coverage consistent with our prediction of zero at $T=0$. Finally, measurements, also very recent, of third-sound propagation in ^{4}He on Cs-coated glass by Ketola, Wang, and Hallock[33] find that the sound does not propagate when the ^{4}He vapor pressure is such that ^{4}He adsorption on bare glass is less than nine layers. The sound does propagate when this thickness is greater than 11.5 layers, and there is hysterisis between 9 and 11.5 layers. This result is consistent with our prediction and the results of Ref. 62 if (1) there were sufficient surface impurities, e.g., oxygen, promoting wetting by increasing the effective well depth D to just above the wetting-nonwetting line in Fig. 1, or (2) the Cs surface, having area A_s, was rather rough, enhancing its associated surface energies by a factor A_s/A, where A is the area of the (flat) liquid-vapor interface. In the latter case, the nonwetting region is determined by (assuming that the length scales associated with the roughness are large compared to atomic scales),

$$\sigma_{\rm sl} \geq \sigma_{\rm sv} + \left[\frac{A}{A_s} \right] \sigma_{\rm lv} \; . \tag{2.30}$$

The factor $(A/A_s) < 1$ allows one to violate the inequality at smaller D than for the case of no roughness since $\sigma_{\rm sl}$ is a decreasing function of D.

Nacher and Dupont-Roc observed wetting on Rb, K, and Na. Wetting on Rb and K disagrees with our predictions. There are both experimental and theoretical uncertainties which could resolve the discrepancies. As noted by the experimentalists, oxides, which were inevitably present to some unknown degree, would favor wetting when it would otherwise not occur. On the other hand, the detailed theoretical predictions for specific elements are subject to uncertainties in the values of the potential parameters employed; see Table I. These are, in fact, theoretical values, as there exist no experimental data pertinent to He adsorption on the alkali metals. Published theoretical values for D differ by as much as 50%, while those for C_3 differ by up to 10%.[12] Under these circumstances, our quantitative predictions for specific substrates, but not the qualitative trends, are necessarily uncertain.

Behavior qualitatively similar to that of ^{4}He is expected for the heavier noble gases, but the interaction parameters are not well known. Indeed, there are experimental data[63] which have been interpreted[64] as implying that Xe and Ar do not wet potassium-coated Ni(100) but do wet the bare surface. There is evidence that Kr does not adsorb significantly on Na.[65] Finally, recent work[66] indicates that none of the heavier rare gases, Ne through Xe, wets Li, Na, or K-plated Ru(001), although they do wet bare Ru.

It is important to assess the observability[25] of prewetting within our theory, given that prewetting transitions have proven so notoriously difficult to observe in classical systems.[26] We find that prewetting typically occurs at $\Delta\mu \sim -1$ K. While our calculations are strictly applicable only at $T=0$, we can assume that at low temperatures the phase diagram will be similar to that at $T=0$, so that prewetting would occur at a ^{4}He vapor pressure P given by the ideal-gas result $P = P_0 \exp(\Delta\mu/T) \leq P_0/2.7$ for $T \leq 1$ K. Thus, P is expected to be substantially separated from P_0 and should be readily observable. A plot of the magnitude of the prewetting jump Δl (in layers) is given in Fig. 6 as a function of D for fixed $C_3 = 1000$ K Å^3. Note again that Δl is infinite at the wetting-nonwetting boundary (at $D = D_0 = 9.6$ K) and appears to saturate at a value of about 0.4 layer for large D. Shirron and Mochel[31] have recently measured adsorption isotherms and third-sound velocities for ^{4}He adsorbed on H_2. Near $P/P_0 = 0$ they observe a rapid rise in coverage at $T = 0.8$ K to about 0.5 layers. For H_2 at $T=0$ we find a prewetting jump of 0.43 layers at $\Delta\mu = -3.59$ K. Using the ideal-gas result just quoted at $T = 0.8$ gives $P/P_0 = 0.01$. Thus both the observed coverage jump and the pressure range over which it occurs appear consistent with our prewetting predictions for ^{4}He on H_2. A very recent, more detailed, study by Chen and Mochel[67] of third sound and heat capacity in the submonolayer region has indicated the presence of a new phase transition here, most likely a prewetting transition. If further studies at very low P/P_0 confirm this picture, prewetting will have been seen for the first time since its prediction in 1977.[26] Recent precision measurements by Greywall and Busch[68] of the heat capacity of ^{4}He on a graphite surface in each of the first three layers indicate the presence of a 2D liquid (which solidifies with further coverage in the first two layers but probably not in the third) with a density of about 0.04 Å^{-2}, essentially identical with our saturation value at large D of Δl in Fig. 6. We interpret the third-layer 2D liquid-gas transition as the closest analog of prewetting in the weak-binding case. The predicted prewetting jump of 5.25 layers on Na is rather large and should be readily observable. We expect that the thin films at prewetting transitions, which have zero thickness at $T=0$, will have increasing nonzero thicknesses as a function of T.

Substrates such as H_2, Ne, and Ar, which are less weak binding than the alkali metals, have received recent experimental attention.[62,49,69,70,31] The case of a H_2 substrate, falling on the wetting side of the wetting-nonwetting borderline of Fig. 1, is of particular interest. Recent experiments[69,70,31] show that ^{4}He wets H_2. Further, the third-sound experiments[31] show an oscillatory structure qualitatively similar to our theoretical one of Fig. 12. However, we observe a periodicity of one layer, as opposed to the half-layer periodicity of Ref. 31. As far as we know, no mechanism has been proposed to explain half-layer periodicity. Indeed, the third-sound data of Zimmerli and Chan[58] for the case of a H_2 bilayer on graphite show oscillations with the expected periodicity.

Experiments on compound substrates would appear to be a fertile area for future investigation. In particular, the case of ^{4}He adsorbed on Cs-preplated graphite (see Table II), is the case where a crossover from wetting to nonwetting as a function of increasing Cs thickness can be confidently predicted.

Similarly of interest are porous media which present weak-binding surfaces. Relative to the planar case, the energy balance is altered by the modified potential field and the possible absence of a liquid-vapor interface, in the capillary-condensed phase. For instance, the analog of the left-hand side of Eq. (2.1) in the latter case would be reduced by a factor of 2 for an idealized plane-parallel model of the pore. For very small pores the geometry will also decrease the attractive well depth D.

III. ^{3}He

A qualitative understanding of wetting of liquid ^{3}He can be obtained through the simple Eq. (2.3), which also applies here. Introducing the appropriate values for the surface tension and equilibrium density, the nonwetting condition becomes

$$(C_3D^2)^{1/3} \leq 23 \text{ K Å} . \tag{3.1}$$

The lowest value of the left-hand side of this equation, obtained from the data of Fig. 1, is about 24 K Å for Cs, implying that this case, and only this case, is marginally a candidate for nonwetting. However, Eq. (3.1) provides too strong a constraint, because it assumes that the fluid energy associated with the formation of the interface with the substrate is the same as for the free surface, whereas it is actually greater. Indeed, the free-surface profile minimizes the surface tension, so any perturbation of this profile, e.g., that produced by the substrate potential, will cost more energy. Hence the nonwetting line lies certainly above that given by Eq. (3.1), as is seen for the ^{4}He case in Fig. 1. The question is now to estimate whether it is sufficiently far above in order that some of the alkali metals lie in the nonwetting region.

A nonlocal functional for pure ^{3}He can be constructed along the same line as for ^{4}He (Ref. 23) or helium mixtures.[24] Surface properties using such a functional have been calculated in Ref. 71, where it was shown that the actual surface tension is correctly reproduced; a related approach, starting from the pseudopotential theory of Pines and co-workers, can be found in Ref. 72. In the following, we investigate wetting of liquid ^{3}He within the framework of Ref. 71, which we now briefly recall.

The ground-state wave function is chosen as a Slater determinant of single-particle states Φ_i, to be determined self-consistently. The energy of the fluid is written as

$$E = E_{\text{kin}} + E_{\text{pot}} \tag{3.2a}$$

with

$$E_{\text{pot}} = \tfrac{1}{2} \int \rho(\mathbf{r}) V_l(\mathbf{r}-\mathbf{r}') \rho(\mathbf{r}') d\mathbf{r}\, d\mathbf{r}' + \frac{c_3}{2} \int \rho(\mathbf{r}) [\bar{\rho}(\mathbf{r})]^{\gamma} d\mathbf{r} , \tag{3.2b}$$

$$\rho(\mathbf{r}) = \sum_i |\Phi_i(\mathbf{r})|^2 . \tag{3.2c}$$

For the long-range part, we take of course the same Lennard-Jones interatomic potential, screened at distances shorter than a distance h_3 (different from that used for ^{4}He) by the same fourth-power law. The "coarse-grained" density $\bar{\rho}(\mathbf{r})$ entering the density-dependent component is obtained by averaging the point density over a sphere of radius h_3.

The kinetic-energy term contains a density-dependent effective mass m^*

$$E_{\text{kin}} = \int \frac{\hbar^2}{2m^*(\mathbf{r})} \tau(\mathbf{r}) d\mathbf{r} , \tag{3.3a}$$

$$\tau(\mathbf{r}) = \sum_i |\nabla \Phi_i(\mathbf{r})|^2 , \tag{3.3b}$$

$$\frac{\hbar^2}{2m^*(\mathbf{r})} = \frac{\hbar^2}{2m_3} \left[1 - \frac{\bar{\rho}(\mathbf{r})}{\rho_c} \right]^2 , \tag{3.3c}$$

where m_3 denotes the bare mass of a ^{3}He atom.

The functional so defined depends on four parameters, the values of which are determined by asking that four properties of the liquid be correctly reproduced, namely the energy per particle, the compressibility and the density at saturation, and the effective mass. The resulting values are

$$h_3 = 2.356 \text{ Å} , \tag{3.4a}$$

$$c_3 = 1\,405\,057 \text{ K}^{1+\gamma} , \tag{3.4b}$$

$$\gamma_3 = 2.1 , \tag{3.4c}$$

$$\rho_c = 0.0406 \text{ Å}^{-3} . \tag{3.4d}$$

With these parameters, the equation of state and the density dependence of the effective mass are accurately reproduced up to solidification pressure.

The reduction to a planar geometry is done in the same way as for pure ^{4}He. The eigenstates are now labeled by a 2D momentum $\mathbf{k}$ parallel to the substrate and a momentum k_z perpendicular to it. Minimizing the energy of the system under the constraint of normalized wave functions leads to a set of coupled Hartree-Fock-like equations,

$$-\frac{\hbar^2}{2m^*(z)} \frac{d^2\Phi(z)}{dz^2} - \frac{d}{dz} \left[\frac{\hbar^2}{2m^*(z)} \right] \frac{d\phi(z)}{dz} + \left[\frac{\hbar^2}{2m^*(z)} k^2 + U_{\text{nl}}(z) + V(z) \right] \Phi(z) = \epsilon_{k,k_z} \Phi(z) . \tag{3.5}$$

The Lagrange multipliers ϵ_{k,k_z} appear as the single quasiparticle energies. Their values are imposed by the bulk liquid far from the substrate. The substrate potential V_{ext} is given in Eq. (2.2), and U_{nl} is given by Eq. (2.16) with the substitutions $h \rightarrow h_3$, $\gamma \rightarrow \gamma_3$, and $c \rightarrow c_3$. The free energy associated with the formation of the interface with the substrate is given by

$$\sigma = E_{\text{kin}} + E_{\text{pot}} + \int \rho(z) V(z) dz - \epsilon_F \int \rho(z) dz , \tag{3.6}$$

where ϵ_F is the Fermi energy. Details of the solution of the set of Eq. (3.5) can be found in Ref. 71.

Figure 15 shows the resulting position of the wetting-nonwetting line in the (C_3, D) plane. As expected, it lies above the simple estimate of Eq. (3.1). Cesium is the only substance clearly in the nonwetting region, Rb being right on the borderline. The Cs value of σ is -0.043 K Å^{-2}, corresponding to a contact angle of 68°. The computation of the wetting-nonwetting line assumes that, as for ^{4}He, the wetting transition is from a film of zero thickness to one of infinite thickness.

For purposes of comparison, we display in Fig. 16 the infinite film profiles for both ^{3}He and ^{4}He on K. As expected, the Fermi character of ^{3}He produces more pronounced density oscillations than those obtained for ^{4}He.

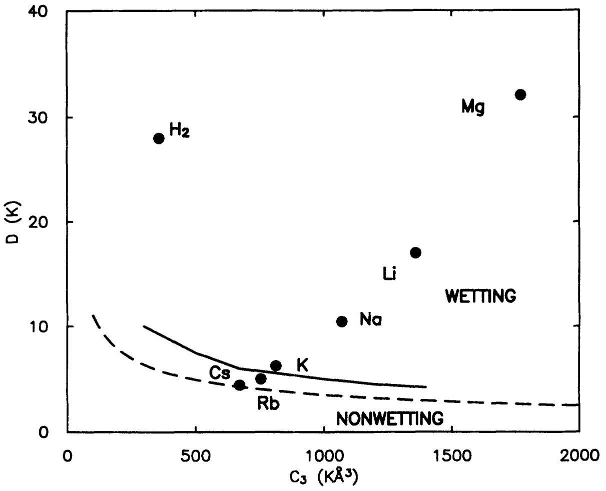

FIG. 15. Phase diagram for ^{3}He adsorption on weak-binding substrates showing the wetting-nonwetting line from the nonlocal theory (solid curve). The dashed-dotted curve uses the more simplistic estimate, based on Eqs. (2.1) and (3.1).

An interesting question to consider at this point is that of prewetting transitions in thin films. A detailed discussion of this point will be given elsewhere, but one can present here some tentative remarks. In the case of ^{4}He, we have seen that the prewetting jump predicted for moderately attractive substrates reflects the fact that a strong-binding substrate constrains thin films to a 2D geometry and that 2D ^{4}He, in the present approach as in others,[73] is found to be a liquid. To the contrary, 2D ^{3}He is expected to be a gas[73]; this is also found in the present model and we expect such a behavior in thin films—in contrast to the case of ^{4}He. Indeed, its reduction to 2D gives

$$\omega=\frac{\hbar^2}{2m}\left[1-\frac{3}{4h_3}\frac{\rho_{2D}}{\rho_c}\right]^2\pi\rho_{2D}^2+\frac{4\pi}{3}\epsilon\sigma^2\rho_{2D}^2\left[\frac{8}{5}\left[\frac{\sigma}{h_3}\right]^{10}-\frac{5}{2}\left[\frac{\sigma}{h_3}\right]^4\right]+\frac{c_3}{2}\left[\frac{3}{4h_3}\right]^{1+\gamma}\rho_{2D}^{2+\gamma}-\mu\rho_{2D}\,, \tag{3.7}$$

which predicts a single gaseous phase.

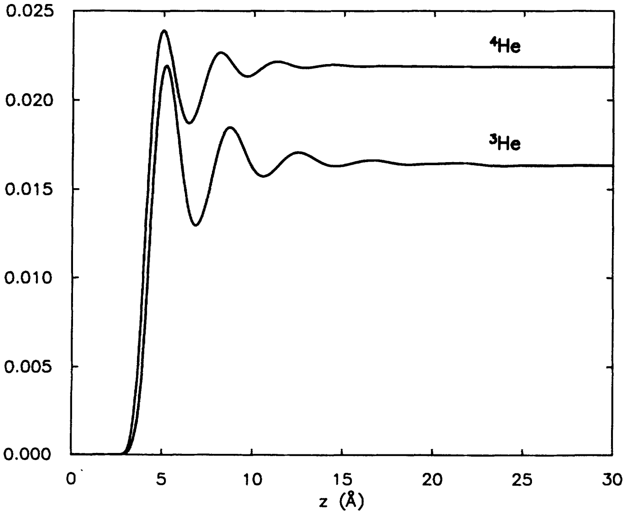

FIG. 16. Density profiles for infinitely thick films of ^{3}He and ^{4}He on K.

However, with increasing thickness, the third dimension begins to play a role, and as more interactions between atoms can now take place, a liquid phase should be favored. This suggests the possibility of a transition between a thin gaseous film and a thicker liquid one. This transition would appear as a prewetting jump between two films of different thicknesses. We anticipate that this transition should disappear at a prewetting critical point for sufficiently attractive substrates. The determination of whether this fascinating 2D gas to thick liquid film transition does occur as well as the thicknesses involved requires the application of the present model to films. Work in this direction is in progress.

IV. DISCUSSION

He films have been shown here to exhibit diverse behavior, depending on the substrate. In many cases, the adsorption potential is strongly attractive. As seen in Figs. 9 and 11, there occurs the formation of one or more solid layers, followed by complete wetting by liquid He. Other possible kinds of behavior arise if the well depth *D* is small; these include continuous wetting without solidification or two more interesting possibilities: nonwetting and prewetting. Until recently the former had not been observed or predicted for He and the latter had not been observed for any adsorption system. Experiments[31,32,33,61] stimulated in part by our work[35,36] have shown our predictions to be at least qualitatively reliable. Certainly further experiments are needed to resolve these questions.

On the theoretical side, many issues remain to be addressed. Firstly, reliable potentials are urgently needed; without these, accurate predictions are not possible. Further, more accurate techniques, such as Green's function and path-integral Monte Carlo, should be brought to bear, given the fundamental importance of these phenomena. Of particular interest, in our opinion, are questions about the presence and character of superfluid transitions for these systems. In principle, the corrugation of the substrate potential ought to be included because of the role of epitaxial effects in solid phases. Finally, particular interest ought to be drawn, both experimentally and theoretically, to the problem of ^{3}He-^{4}He mixtures. Past experiments have revealed strong preferential adsorption of ^{4}He, because the higher density maximizes its potential-energy gain. In the weak-binding case studied here, in contrast, the ^{3}He may segregate to the substrate because of its lower surface energy. One of the more intriguing possibilities we predict is a ^{4}He "sandwich"; one

^{3}He monolayer resides near the substrate and another resides at the film-vapor interface. Conceivably, a high-T_c superfluid state may ensue as a result of the coupling between the layers.[74]

Note added. After this work was completed we received work from P. Taborek and J. E. Rutledge [P. Taborek and J. E. Rutledge, Phys. Rev. Lett. **68**, 2184 (1992); J. E. Rutledge and P. Taborek (unpublished).] describing experimental results for ^{4}He on Cs in agreement with the phase diagram sketched in Fig. 13(b). This work provides evidence for the observation of conventional[25] prewetting.

ACKNOWLEDGMENTS

Thanks are due to several individuals for helpful comments and discussions. These include Moses Chan, Bob Hallock, Jay Maynard, Jack Mochel, Oscar Vilches, Greg Dash, Michael Schick, Tim Sluckin, Michael Swift, Bob Guyer, and David Edwards. This work was partially supported by Ohio State University and by NSF Grants No. DMR-9022681 and No. DMR-9014679. Part of the numerical calculations reported here were made possible through an Ohio Supercomputer Center grant.

APPENDIX

Here we give a derivation of the low-temperature limit of the third-sound velocity which is independent of the detailed structure of the film. For a conventional derivation see, e.g., Ref. 51. We start with the continuity equation, which is well-defined microscopically,

$$\frac{\partial\rho}{\partial t}=-\nabla\cdot\mathbf{g}\ , \tag{A1}$$

where $\mathbf{g}$ is the mass current. Assuming that any normal fluid is clamped, $\mathbf{g}=\rho_s v_s$, where $\mathbf{v}_s$ is the superfluid velocity and ρ_s is the superfluid density. Linearizing and assuming that any flow is parallel to the substrate allows us to write $\mathbf{g}=\rho_s^0(z)\mathbf{v}_s(\mathbf{r}_\parallel)$, where $\rho_s^0(z)$ is the unperturbed superfluid density depending only on the coordinate z normal to the substrate, and $\mathbf{r}_\parallel$ is the position vector in the plane of the substrate. We next integrate Eq. (A1) over z to obtain

$$\frac{\partial n}{\partial t}=-n_s\nabla_\parallel\cdot\mathbf{v}_s\ , \tag{A2}$$

where

$$n=\int\rho\,dz \tag{A3}$$

and

$$n_s=\int\rho_s^0 dz\ . \tag{A4}$$

Next we recall[75] that the superfluid velocity is related to the gradient of the phase ϕ of the condensate wave function by

$$\mathbf{v}_s=\frac{\hbar}{m}\nabla_\parallel\phi\ , \tag{A5}$$

where

$$\frac{\partial\phi}{\partial t}-\mu/\hbar\ . \tag{A6}$$

Note that the assumption that flow is parallel to the substrate is equivalent to the assumption that ϕ depends only on $\mathbf{r}_\parallel$ and t. Combining Eqs. (A5) and (A6) gives

$$\frac{\partial\mathbf{v}_s}{\partial t}=-\nabla\mu/m\ . \tag{A7}$$

Finally, a combination of Eqs. (A2) and (A7), assuming that μ is a local function of the density only, gives

$$\frac{\partial^2 n}{\partial t^2}=\frac{n_s}{m}\frac{\partial\mu}{\partial n}\nabla^2 n\ , \tag{A8}$$

from which the third-sound velocity c_3 emerges as

$$c_3^2=\frac{n_s}{m}\frac{\partial\mu}{\partial n}\ . \tag{A9}$$

In the limit of a 2D film, $c_3=[n_s/n]^{1/2}c_l$, where c_l is the speed of longitudinal sound in 2D.

---

[1] J. G. Daunt and K. Mendelssohn, Proc. R. Soc. London Ser. A **170**, 439 (1939).

[2] D. F. Brewer, in the *Physics of Liquid and Solid Helium,* edited by K. H. Bennemann and J. B. Ketterson (Wiley, New York, 1978), Part II, p. 573.

[3] D. R. Tilley and J. Tilley, *Superfluidity and Superconductivity* (Hilger, Bristol, 1974).

[4] I. E. Dzyaloshinskii, E. M. Lifshitz, and L. P. Pitaevskii, Adv. Phys. **10**, 165 (1961).

[5] E. S. Sabisky and C. H. Anderson, Phys. Rev. A **7**, 790 (1973).

[6] E. Cheng and M. W. Cole, Phys. Rev. B **38**, 987 (1988) and references therein.

[7] J. M. Kosterlitz and D. J. Thouless, in *Progress in Low Temperature Physics,* edited by D. F. Brewer (North-Holland, Amsterdam, 1978), Vol. VII B, p. 371.

[8] J. C. Davis, A. Amar, J. P. Pekola, and R. E. Packard, Phys. Rev. Lett. **60**, 302 (1988).

[9] H. Godfrin, R. R. Rueland, and D. D. Osheroff, Phys. Rev. Lett. **60**, 305 (1988).

[10] S. Ramesh, Q. Zhang, G. Torzo, and J. D. Maynard, Phys. Rev. Lett. **52**, 2375 (1984).

[11] D. A. Huse, Phys. Rev. B **29**, 6985 (1984).

[12] A review of adsorption potentials is given by G. Vidali, G. Ihm, H. Y. Kim, and M. W. Cole, Surf. Sci. Rep. **12**, 133 (1991).

[13] Equation (1.2) assumes the vapor to be ideal.

[14] Deviation from Eq. (1.3) is significant at $d\geq 100$ Å. For thickness $d\geq 10^3$ Å, $f(d)\propto d^{-4}$; see Refs. 4 and 6 for a discussion of these regimes.

[15] S. Dietrich, in *Phase Transitions and Critical Phenomena,* edited by C. Domb and J. L. Lebowitz (Academic, New York, 1987), Vol. 12.

[16] Many-body and collective electron effects are omitted. See L. W. Bruch, Surf. Sci. **125**, 194 (1983).

[17] See W. A. Steele, *Interaction of Gases with Solid Surfaces* (Pergamon, Oxford, 1974), p. 34.

[18] R. A. Aziz, in *Inert Gases,* edited by M. L. Klein (Springer-Verlag, Berlin, 1984).

[19] G. Scoles, Int. J. Quantum Chem. **24**, 475 (1990); B. V. Derjaguin, N. V. Churaev, and V. M. Muller, *Surface Forces* (Consultants Bureau, New York, 1987), p. 88.

[20] See Figs. 2.2–2.4 of Ref. 17.

[21] G. Ihm, M. W. Cole, F. Toigo, and J. R. Klein, Phys. Rev. A **42**, 5244 (1990).

[22] G. Scoles, Annu. Rev. Phys. Chem. **31**, 81 (1980).

[23] J. Dupont-Roc, M. Himbert, N. Pavloff, and J. Treiner, J. Low Temp. Phys. **81**, 31 (1990).

[24] N. Pavloff and J. Treiner, J. Low Temp. Phys. **83**, 331 (1991).

[25] Prewetting conventionally (Refs. 15, 29, and 30) refers to a line of first-order transitions in film thickness (thin-thick transitions) terminating at coexistence in a first order, thermally driven wetting transition. Our usage involves a natural generalization of this to the case where the first-order wetting transition can be driven by any variable change, in particular by changes in the potential parameters C_3 and D, as well as T. In this situation a prewetting transition P_w at $T=0$ can occur off coexistence, the associated wetting transition at coexistence being reached by varying the potential (e.g., by varying the Cs concentration in a Cs-Mg alloy substrate).

[26] C. Ebner and W. F. Saam, Phys. Rev. Lett. **38**, 1486 (1977).

[27] J. W. Cahn, J. Phys. Chem. **66**, 3667 (1977).

[28] J. Finn and P. A. Monson, Phys. Rev. A **39**, 6402 (1989).

[29] D. E. Sullivan and M. M. Telo da Gama, in *Fluid Interfacial Phenomena,* edited by C. A. Croxton (Wiley, New York, 1986), p. 45.

[30] See, e.g., M. Schick, in *Liquids and Interfaces,* edited by J. Charvolin, J. F. Joanny, and J. Zinn-Justin, 1988 Les Houches, Session XLVIII (Elsevier, New York, 1990).

[31] P. J. Shirron and J. M. Mochel, Phys. Rev. Lett. **67**, 1118 (1991).

[32] S. K. Mukherjee, D. P. Druist, and M. H. W. Chan (unpublished).

[33] K. S. Ketola, S. Wang, and R. B. Hallock, Phys. Rev. Lett. **68**, 201 (1992).

[34] E. Cheng, G. Ihm, and M. W. Cole, J. Low Temp. Phys. **74**, 519 (1989).

[35] E. Cheng, M. W. Cole, W. F. Saam, and J. Treiner, Phys. Rev. Lett. **67**, 1007 (1991).

[36] E. Cheng, A. Chizmeshya, M. W. Cole, J. R. Klein, J. Ma, W. F. Saam, and J. Treiner, Physica A **177**, 466 (1991).

[37] Interesting submonolayer behavior on weak-binding substrates is discussed in Ref. 36, in E. Cheng, M. W. Cole, and P. B. Shaw, J. Low Temp. Phys. **82**, 49 (1991), and in J. F. Annett, M. W. Cole, P. B. Shaw, and R. M. Stratt, J. Low Temp. Phys. **84**, 1 (1991).

[38] See, e.g., N. Nakanishi and M. E. Fisher, Phys. Rev. Lett. **49**, 1565 (1982) for a clear depiction of prewetting sheets.

[39] For $\beta<2.2$ two transitions in film thickness appear, one of them possessing a prewetting critical point. For $1.57<\beta<2.2$ the corresponding transition lines meet in a triple point in α-h space, while for $\beta<1.57$ the two lines are separate.

[40] A lack of translational invariance, of course present for all physical substrates, will have the effect of somewhat reducing the superfluid fraction below unity, even at $T=0$. See, e.g., M. P. A. Fisher, P. B. Weichman, G. Grinstein, and D. S. Fisher, Phys. Rev. B **40**, 546 (1989).

[41] Local functionals of the Skyrme type have been extensively employed to describe properties of atomic nuclei. See D. Vautherin and D. M. Brink, Phys. Lett. **32B**, 149 (1970); M. Beiner, H. Flocard, Nguyen Van Giai, and P. Quentin, Nucl. Phys. **A238**, 29 (1975).

[42] P. Tarazona, Phys. Rev. A **31**, 2672 (1985).

[43] P. A. Whitlock, G. V. Chester, and M. H. Kalos, Phys. Rev. B **38**, 2418 (1988), and references therein.

[44] The force constant of the potential in Eq. (2.2) is $18C_3(3D/2C_3)^{5/3}$.

[45] E. Kortscheck, G.-X. Qian, and W. Kohn, Phys. Rev. B **31**, 4245 (1985); E. Kortscheck, *ibid.* **31**, 4258 (1985); **32**, 5713 (1985).

[46] G. Ji and M. Wortis, Phys. Rev. **34**, 7704 (1986). See also G. Ji, Ph.D. dissertation, University of Illinois, 1986.

[47] M. Bretz, Phys. Rev. Lett. **31**, 447 (1973).

[48] H. J. Lauter, H. P. Schildberg, H. Godfrin, H. Wiechert, and R. Haensel, Can. J. Phys. **65**, 1435 (1987), and references therein.

[49] G. Zimmerli, G. Mistura, and M. H. W. Chan, Phys. Rev. Lett. **68**, 60 (1992).

[50] H. J. Lauter, H. Godfrin, and P. Leiderer (unpublished).

[51] D. Goodstein, Phys. Rev. **183**, 327 (1969).

[52] E. Cheng, M. W. Cole, W. F. Saam, and J. Treiner (unpublished).

[53] See, e.g., D. J. Bishop and J. D. Reppy, Phys. Rev. B **22**, 5171 (1980), and references therein.

[54] D. M. Ceperley and E. L. Pollock, Phys. Rev. B **39**, 2084 (1989).

[55] See, e.g., Refs. 32, 49, and 34.

[56] See, e.g., D. J. Bishop and J. D. Reppy, Phys. Rev. B **22**, 5171 (1980), and references therein.

[57] D. O. Edwards and W. F. Saam, in *Progress in Low Temperature Physics,* edited by D. F. Brewer (North-Holland, Amsterdam, 1978), Vol. VII A, Chap. 4, p. 291.

[58] Rayleigh waves, phonons localized at a solid surface, are essentially two-dimensional and thus have a T^3 free energy. Reflected phonons have a contribution proportional to the three-dimensional free energy, going as T^4, times a phonon thermal wavelength $\lambda_T \sim 1/T$, as the surface disturbs the bulk phonon energy density over a distance of order λ_T; see, e.g., Ref. 57.

[59] C. Ebner and W. F. Saam, Phys. Rev. Lett. **58**, 587 (1987); Phys. Rev. B **35**, 1822 (1987).

[60] W. F. Saam, J. Treiner, E. Cheng, and M. W. Cole, J. Low Temp. Phys. (to be published).

[61] P. J. Nacher and J. Dupont-Roc, Phys. Rev. Lett. **67**, 2966 (1991).

[62] P. J. Shirron, K. A. Gillis, and J. M. Mochel, J. Low Temp. Phys. **75**, 349 (1989); **78**, 157 (1990); (private communication).

[63] D. R. Mullins, J. M. White, and H. S. Luftman, Surf. Sci. **167**, 39 (1986).

[64] M. Onellion and J. L. Erskine, Surf. Sci. **177**, L983 (1986).

[65] R. A. Pierotti and G. D. Halsey, Jr., J. Phys. Chem. **63**, 680 (1959).

[66] D. Menzel (private communication).

[67] M.-T. Chen and J. M. Mochel (unpublished)

[68] D. S. Greywall and P. A. Busch, Phys. Rev. Lett. **67**, 3535 (1991).

[69] M. A. Paalenen and Y. Iye, Phys. Rev. Lett. **55**, 1761 (1985); D. Cieslikowski, A. J. Dahm, and P. Leiderer, *ibid.* **58**, 1751 (1987).

[70] M. H. W. Chan (private communication). See also G. J. van den Borg, in *Proceedings of the International Conference on Low Temperature Physics,* Oxford, 1951, edited by R. Bowers (North-Holland, Amsterdam, 1990).

[71] J. Treiner (unpublished)

[72] S. Weisberger and P. G. Reinhardt, Phys. Lett. A **158**, 407 (1991).

[73] M. D. Miller and L. H. Nosanow, J. Low Temp. Phys. **32**, 145 (1978).

[74] This is analogous to the sandwich geometry advocated by V. L. Ginzburg, Phys. Lett. **13**, 101 (1964) to increase the superconducting transition temperature.

[75] See, e.g., P. Nozières and D. Pines, *Theory of Quantum Liquids, Vol. II* (Addison-Wesley, Reading, MA, 1988).

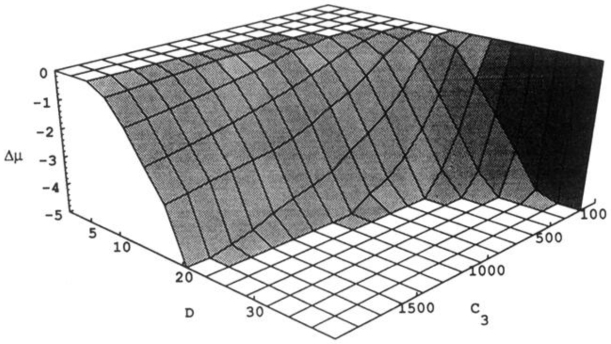

FIG. 5. Prewetting transition sheet, terminating in the wetting-nonwetting transition in the C_3-D plane. D and μ are in K, C_3 in K Å^3.